Available online at www.sciencedirect.com
SCIENCE DIRECT®
Journal of Sound and Vibration 291 (2006) 369–387
JOURNAL OF SOUND AND VIBRATION
www.elsevier.com/locate/jsvi

An improved method for the reconstruction of a distributed force acting on a vibrating structure ☆

Yi Liu, W. Steve Shepard Jr.*

Department of Mechanical Engineering, The University of Alabama, 290 Hardaway Hall, Box 870276, Tuscaloosa, AL 35487-0276, USA

Received 8 March 2004; received in revised form 12 May 2005; accepted 14 June 2005
Available online 24 August 2005

Abstract

Indirectly reconstructing distributed forces from measured structural response is necessary when the direct measurement of these dynamic forces is not possible. An improved method for reconstructing distributed forces is developed in this paper. Unlike the traditional modal method for force reconstruction, the forcing spatial function is decomposed only over the known forcing region. Numerical simulations illustrate that when compared with the traditional modal method, this new method tends to obtain better reconstruction results while requiring fewer basis functions. A theoretical proof is provided to reveal the applicability and limitations of this new method. It turns out that this approach, like other inverse methods, can also be an ill-posed method. To address this issue, a regularization process is introduced to increase the inverse stability. Numerical results show that when the regularization process is applied to simulated response measurements that include noise, the new method is able to reconstruct spatially distributed external forces with improved accuracy.

☆ Portions of this work were presented in 'An Improved Spatial Operational Force Reconstruction Method', The 22nd Southeastern Conference on Theoretical and Applied Mechanics, Tuskegee, AL, August 2004.

*Corresponding author. Tel.: +1 205 348 0048; fax: +1 205 348 6419.
E-mail address: sshepard@coe.eng.ua.edu (W.S. Shepard Jr.).

0022-460X/$ - see front matter © 2005 Elsevier Ltd. All rights reserved.
doi:10.1016/j.jsv.2005.06.013

1. Introduction

In characterizing the dynamic response of a structure, it is often desirable to know the dynamic forces within the system. For a simple structure being tested in the lab, the force may be considered as that due to an external shaker. In this case, one may use a force sensor between the shaker and structure to measure the imposed force. When the force at a connection between two substructures is of interest, though, the ability to measure these forces can only be achieved for a few specific cases. For many structures, the introduction of a force sensor into the system can upset the dynamic characteristics of the structure. As a result, the presence of the sensor affects the force being measured. Furthermore, the installation of force sensors is often not feasible due to geometric issues. To provide a means for determining the dynamic force when these measurement limitations are present, various methods have been developed for indirectly computing the dynamic forces from a measured response of structural motions. See Ref. [1] for an overview of these approaches and Refs. [2–4] for more recent improvements to these approaches. Although these methods have been shown to be convenient for a wide array of applications, there are some basic assumptions that one must make when using these approaches.

The force reconstruction approaches developed thus far have various limitations when it comes to characterizing the nature of the dynamic force. The primary limitation is the fact that most of the approaches are limited to determining forces that are assumed to act at a single point on the structure. When one is interested in the spatial nature of a force, such as at higher frequencies or for more complex structural connections, these reconstruction approaches have very limited usage. Cremer et al. [5] has shown in the study of an infinite plate that the point force assumption is only valid when the dimensions of the contact region are less than approximately one-tenth of the wavelength. At higher frequencies, the dimensions of the connection become comparable to the wavelength and the force over the contact region can no longer be assumed to be uniform. Consequently, a method for indirectly reconstructing spatially varying forces from measured structural responses is needed. Two reconstruction approaches, based on the finite difference method and the traditional modal method, have been developed to characterize distributed dynamic forces [6]. The finite difference scheme requires a very accurate model of the structure, including the governing differential equations and the boundary conditions. In most engineering problems, the structures are so complicated that it is extremely difficult to formulate the governing equations. Additionally, it is difficult to obtain an accurate description of the boundary conditions for many cases. The other approach addressed in the above-mentioned work is referred to here as the traditional modal approach. The traditional modal approach enables one to calculate the distributed forces by projecting both the distributed force and the response functions into the structural modal space, which is spanned by the structural modal functions. Although this method does enable one to indirectly measure a spatially distributed force, a set of functions that span the entire structure are used to describe a force that only spans over the contact region. As a result, a prohibitively large number of basis functions is often needed to represent the forcing function with acceptable accuracy. Consequently, this approach can be quite inefficient and is often not practical.

To overcome the difficulties noted above, the research presented here describes the development of an improved force reconstruction method that allows a more accurate estimation of the distributed excitation force while requiring fewer basis functions to describe that force.

A theoretical development is first presented and then numerical examples are provided to illustrate the validity of this new experimental approach. Note this new method is developed with the assumption that the excitation region is known a priori and the excitation force is a distributed harmonic force. Nevertheless, the method could be extended to include multiple frequencies.

In the course of describing this new approach, it will be shown that the new method is an ill-posed process, just like the traditional modal method [6]. Ill-posed problems for the inverse process occur, as defined in Ref. [7], when the singular values decay gradually to zero and the ratio between the largest and the smallest nonzero singular values is large. It is well-known that the ill-posed problem can lead to inverse instability [8]. To address the potential problems associated with instabilities in the new approach developed here, a regularization method is implemented. The regularization method allows one to obtain a stable solution by adding appropriately selected side constraints to the inverse formulation [8].

The primary focus of this work is to describe the formulation of the new spatial force reconstruction method and compare this method with the traditional modal method noted above. To that end, a brief review of the traditional modal method is given in the next section. Then, the theoretical development and applicability proof are presented for the new method. Following the discussion pertaining to the application of this new method, the regularization methods used to increase inverse stability are discussed. Finally, some conclusions related to the application of the method are presented. This work provides the development and study of a new method that will be experimentally validated for a real structure in a future work.

2. Traditional modal method

This section provides an overview of the traditional modal force reconstruction method. Although details associated with this method can be found in another work [6], a brief overview of the technique is provided here for completeness and comparison purposes.

Suppose an external distributed conphase dynamic force, $f(\mathbf{x}, t)$, excites an arbitrary structure as illustrated in Fig. 1. As in other works, the term "conphase" is used here to refer to a distributed harmonic force for which each excitation point reaches the maximum or minimum value at the same time. Also the coordinate vector $\mathbf{x}(x, y, z)$ defines a point on the structure, and t denotes time. The relationship between the external dynamic force and the resulting vibratory response, denoted $v(\mathbf{x}, t)$, can be written in the form

$$£[v(\mathbf{x}, t)] = f(\mathbf{x}, t), \tag{1}$$

where $£[\cdot]$ is a linear differential operator, and $v(\mathbf{x}, t)$ can be any physical quality, such as acceleration, velocity, displacement, strain, or stress. For the sake of simplicity in this work, $v(\mathbf{x}, t)$ will be used to denote the displacement. According to general modal theory [9], the response $v(\mathbf{x}, t)$ can be expressed as a linear combination of modal shape functions

$$v(\mathbf{x}, t) = \sum_{i=1}^{\infty} \varphi_i(\mathbf{x}) q_i(t), \tag{2}$$

where $\varphi_i(\mathbf{x})$ denotes the ith normalized mode shape function of the structure, and $q_i(t)$ is the generalized modal coefficient. Suppose there is no damping in the structure for the sake of

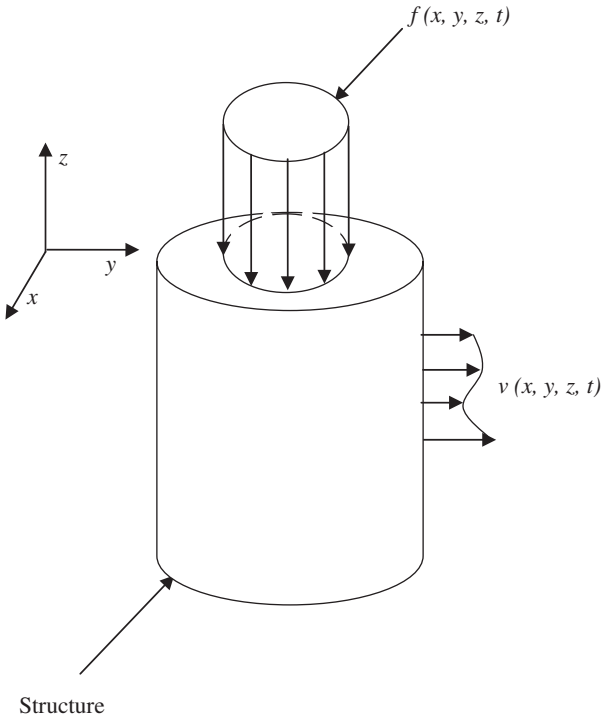

Fig. 1. Structure excited by a distributed force $f(x, y, z, t)$.

simplicity. By substituting Eq. (2) into Eq. (1) and using the orthogonal property of modal functions, one can obtain the generalized equations of motion based on a structural modal description as

$$m_i\left[\ddot{q}_i(t) + \omega_i^2 q_i(t)\right] = \langle f, \varphi_i \rangle, \tag{3}$$

where the modal mass m_i, is defined as

$$m_i = \int_\Omega \rho(\mathbf{x}) \cdot (\varphi_i(\mathbf{x}))^2 \, \mathrm{d}\Omega, \tag{4}$$

$\rho(\mathbf{x})$ denotes the localized mass density of the structure and ω_i is the ith natural frequency. The structure is defined to exist only over the domain Ω. The right-hand-side term of Eq. (3), which describes the coupling between the forcing function and the modal functions, is defined as

$$\langle f, \varphi_i \rangle = \int_\Gamma f(\mathbf{x}, t)\varphi_i(\mathbf{x}) \, \mathrm{d}\Gamma, \tag{5}$$

where Γ is the excitation area. Since the interest here is a conphase distributed force with a harmonic dependence, this force can be represented in complex form as

$$f(\mathbf{x}, t) = \mathrm{Re}\left(F(\mathbf{x})\mathrm{e}^{\mathrm{j}(\omega t)}\right), \tag{6}$$

where $\mathrm{Re}(\cdot)$ denotes the real part of the function, and ω is the circular frequency of excitation. Note that $f(\mathbf{x}, t)$ is a conphase distributed force; hence it is always possible to select a beginning

time such that $F(\mathbf{x})$ is a real-valued magnitude function that only depends on position. Substituting Eq. (6) into Eq. (5), the contribution of the spatial force component that excites the ith spatial mode is obtained. Substituting the result into Eq. (3), one is able to obtain the traditional modal formulation

$$m_i \cdot \left[-\omega^2 + \omega_i^2\right] \cdot q_i(t) = \mathrm{Re}\left(\langle F, \varphi_i \rangle e^{j(\omega t)}\right). \tag{7}$$

For a known excitation, Eq. (7) can be used to determine the contribution of each mode shape, q_i, to the overall response. On the other hand, if one does not know the nature of the excitation, one can first measure the response of the structure and determine the contribution of each mode, q_i, to that overall response [10]. Then, if the modal masses and natural frequencies are known, Eq. (7) can be used to determine the value of $\langle F, \varphi_i \rangle$. Although the value of the integral in Eq. (5) is known, $F(\mathbf{x})$ is still an unknown. If, however, a linear combination of the mode shapes is used to describe the force, then the spatial nature can be found using the expansion

$$F(\mathbf{x}) = \sum_i^{\infty} \langle F, \varphi_i \rangle \varphi_i, \tag{8}$$

where $\langle F, \varphi_i \rangle$ is found using from Eq. (5). This technique is referred to as the traditional modal method for spatial force reconstruction.

Further examination of Eq. (8) shows that the traditional modal method has several limitations. First, the forcing function is represented over a subspace that is spanned beyond its boundaries by the continuous modal functions φ_i. As a result, if the forcing function is discontinuous, which is usually the case at the boundaries of the forcing region, some spatial information of the external forces is lost. This loss of information is due to the fact that only a limited number of modal functions can actually be used in an implementation. Second, the modal functions have nonzero values over the un-forced region. Even though the forced region is often known a priori, there will be some residual component of the force description that spans over this nonforced region. Furthermore, if the forced region is relatively small compared with the size of the structure, then many modal basis function terms will be needed to describe the spatially varying force with acceptable accuracy, which is impossible for some cases where the structural resonance for a mode is far from the excitation frequency and thus signal-to-noise problems arise. As can be concluded from this discussion, there are some important implementation issues that need to be considered when using the traditional modal approach to indirectly compute the spatial force from a measured response. To overcome these difficulties, the development of a new method is presented in the following section. That method will address the issue associated with region over which the force is defined by removing the restriction that the spatial nature of the force be described using the mode shape basis functions.

3. Improved force reconstruction method

In the improved method for reconstructing spatially varying dynamic forces, the force and response are represented using tailored sets of basis functions. Specifically, the external force and

the resulting response are represented using the expansions

$$F(\mathbf{x}) = \sum_{i=1}^{N} W_i \chi_i(\mathbf{x}) \tag{9}$$

and

$$v(\mathbf{x}) = \sum_{i=1}^{N} W_i \psi_i(\mathbf{x}), \tag{10}$$

respectively. The function $\chi_i(\mathbf{x})$ denotes the ith basis function that spans only the forcing space. W_i is a common weighting coefficient such that $\psi_i(\mathbf{x})$ is the structural response directly resulting from the corresponding forcing basis function $\chi_i(\mathbf{x})$ for each respective i. That is, a force described by $\chi_i(\mathbf{x})$ with a unit amplitude will produce a dynamic response of $\psi_i(\mathbf{x})$ with a unit amplitude. It is worth noting that although a single harmonic dependence is assumed here, this case can be easily extended to multi-harmonic cases if a Fourier transform is applied. Additionally, forces for which W_i vary with time can also be considered. For this case, the force can be treated as conphase for a single time step, and then a Fourier transform can be applied to obtain multiple single harmonic forces. Of course, ψ_i constitutes a subset of the response space for the structure which depends on frequency. It is worth noting that χ_i and ψ_i are not necessarily structural modal functions. Furthermore, once χ_i is specified, each corresponding response function ψ_i can be represented using a summation of structural mode shapes for convenience. As noted above, both the forcing function F and response function v have the same weighting coefficients W_i since the system is assumed to be linear. As a result, once the weighting coefficients are obtained by matching Eq. (10) with a measured structural response, which can be obtained numerically from conventional modal analysis, the external distributed force can be computed directly from Eq. (9). To determine the weighting coefficients W_i, a curve-fitting method

$$\mathbf{GW} = \mathbf{B}, \tag{11}$$

is used, where $\mathbf{G}$ is the Gram matrix, consisting of the terms

$$G_{ij} = \int_{\Omega} \psi_i(\mathbf{x}) \psi_j(\mathbf{x}) \, \mathrm{d}\Omega. \tag{12}$$

The $\mathbf{G}$ matrix simply contains the inner products between ψ_i and ψ_j. Note that the orthogonality property of the ψ_i functions is not guaranteed. In a similar manner, B_i, which is the ith entry of vector $\mathbf{B}$, is the inner products between ψ_i and v, such that

$$B_i = \int_{\Omega} \psi_i(\mathbf{x}) v(\mathbf{x}) \, \mathrm{d}\Omega. \tag{13}$$

Once $\mathbf{G}$ and $\mathbf{B}$ are known, then the basis function coefficients vector can be obtained by inverting $\mathbf{G}$ such that

$$\mathbf{W} = \mathbf{G}^{-1}\mathbf{B}. \tag{14}$$

Once the ψ_i functions have been determined, either through numerical or experimental studies, then the above relationships can be used to compute the $\mathbf{G}$ and $\mathbf{B}$ matrices. Then, by using Eq. (14) to find the W_i weights, the spatial force can be reconstructed from Eq. (9). It is worth

noting that the responses over the excitation area can often be difficult to measure. However, if the structure is relatively thin, such as for a plate, one can still measure the responses on the opposing surface. For thick structures, though, one might use an interpolation method to obtain a good approximation for those responses. Note that these approaches might also be applicable to experiments utilizing the traditional modal method. Unlike the traditional modal force reconstruction method described above, in the new method the χ_i functions are not required to be modal functions. These functions must merely be functions for which a corresponding ψ_i can be found. To make the solution obtainable, however, it must be true that each ψ_i resulting from χ_i is linearly independent of all the other ψ_j that result from the other χ_j. In order to validate the applicability of this method, therefore, it is important to prove the linear independence of each ψ_i resulting from χ_i.

4. Theoretical proof

In order to assure the uniqueness of the solution found with this technique, it is necessary to show the ability to invert the **G** matrix as well as determine the conditions under which the ψ_i functions are linearly independent. First, the issue related to the ability to invert **G** will be addressed. In that discussion, the linear independence of the ψ_i's will be assumed. Once the inversion issue has been addressed, then the conditions under which the linear independence of the ψ_i can be assured will be discussed.

To assure that the **G** matrix can be inverted, it is necessary to prove that **G** is a full rank matrix. Assuming that the n ψ_i's are linearly independent, it can be shown that **G** is not rank-deficient. To do this, the Gram matrix **G** is first written in the expanded form

$$\mathbf{G} = \begin{bmatrix} \mathbf{G}_1 \\ \mathbf{G}_2 \\ \vdots \\ \mathbf{G}_n \end{bmatrix} = \begin{bmatrix} \int_\Omega \psi_1\psi_1 \,\mathrm{d}\Omega & \int_\Omega \psi_1\psi_2 \,\mathrm{d}\Omega & \cdots & \int_\Omega \psi_1\psi_n \,\mathrm{d}\Omega \\ \int_\Omega \psi_2\psi_1 \,\mathrm{d}\Omega & \int_\Omega \psi_2\psi_2 \,\mathrm{d}\Omega & \cdots & \int_\Omega \psi_2\psi_n \,\mathrm{d}\Omega \\ \vdots & \vdots & \ddots & \vdots \\ \int_\Omega \psi_n\psi_1 \,\mathrm{d}\Omega & \int_\Omega \psi_n\psi_2 \,\mathrm{d}\Omega & \cdots & \int_\Omega \psi_n\psi_n \,\mathrm{d}\Omega \end{bmatrix}, \tag{15}$$

where $\mathbf{G}_1, \mathbf{G}_2, \ldots, \mathbf{G}_n$ are row vectors. If **G** is assumed to be rank-deficient, then one may also assume that there exists a vector $\mathbf{G}_i$ that can be represented as a linear combination of $\mathbf{G}_1, \ldots, \mathbf{G}_{i-1}, \mathbf{G}_{i+1} \ldots, \mathbf{G}_n$, such that

$$\mathbf{C} = \mathbf{G}_i - (k_1\,\mathbf{G}_1 + \cdots + k_{i-1}\,\mathbf{G}_{i-1} + k_{i+1}\,\mathbf{G}_{i+1} + \cdots + k_n\,\mathbf{G}_n) = \mathbf{0}, \tag{16}$$

where k_i represents a constant. By substituting the appropriate rows of Eq. (15) into Eq. (16), it can be concluded that

$$\mathbf{C}^{\mathrm{T}} = \begin{bmatrix} \int_\Omega \psi_1\left[\psi_i - k_1\psi_1 - \cdots - k_{i-1}\psi_{i-1} - k_{i+1}\psi_{i+1} - \cdots - k_n\psi_n\right] \mathrm{d}x\,\mathrm{d}y\,\mathrm{d}z \\ \int_\Omega \psi_2\left[\psi_i - k_1\psi_1 - \cdots - k_{i-1}\psi_{i-1} - k_{i+1}\psi_{i+1} - \cdots - k_n\psi_n\right] \mathrm{d}x\,\mathrm{d}y\,\mathrm{d}z \\ \vdots \\ \int_\Omega \psi_n\left[\psi_i - k_1\psi_1 - \cdots - k_{i-1}\psi_{i-1} - k_{i+1}\psi_{i+1} - \cdots - k_n\psi_n\right] \mathrm{d}x\,\mathrm{d}y\,\mathrm{d}z \end{bmatrix} = \begin{bmatrix} 0 \\ 0 \\ \vdots \\ 0 \end{bmatrix}, \tag{17}$$

since the multiplication order in the integrand is not important and the linear combination of the integrals can be rewritten as the integral of the linear combination. The simultaneous equations in Eq. (17) state that each function $\psi_1, \psi_2, \ldots, \psi_n$ is orthogonal with respect to the function $\psi_i - k_1\psi_1 - \cdots - k_{i-1}\psi_{i-1} - k_{i+1}\psi_{i+1} - \cdots - k_n\psi_n$. This statement cannot be valid since $\psi_i - k_1\psi_1 - \cdots - k_{i-1}\psi_{i-1} - k_{i+1}\psi_{i+1} - \cdots - k_n\psi_n$ is in the space of $\{\psi_1, \psi_2, \ldots, \psi_n\}$ and it was originally assumed in this discussion that the n χ_i's are linearly independent. By this contradiction, it can be concluded that if the n ψ_i's are linearly independent, then the **G** matrix is not rank-deficient. Hence, **G** can be inverted. As a result, all of the issues related to this new force reconstruction method hinge on the ability to show that the n ψ_i's are linearly independent. Before providing a proof and stating under what circumstances these conditions are met, though, it is first useful to give some relevant definitions.

The linear span, or closure $\bar{\varphi}$, of a set of structural modal functions $\{\varphi_1, \varphi_2, \ldots\} \subset V_\varphi$, is the set of linear combinations

$$v(x, y, z) = \sum_{i=1}^{\infty} a_i \varphi_i(\mathbf{x}), \tag{18}$$

that are contained in the structural response space V_φ, where the a_i is a constant coefficient. Note that V_φ contains all possible responses regardless of the actual input. Furthermore, χ_i and ψ_i are defined to be in the space

$$\{\chi_1, \chi_2, \ldots\} \subset V_\chi, \tag{19}$$

$$\{\psi_1, \psi_2, \ldots\} \subset V_\psi, \tag{20}$$

where V_χ is the space of the driving force basis functions and V_ψ is the space of the structure responses over the whole structure resulting from the local force χ_i's. Notice that the response space V_ψ must be contained within V_φ such that

$$V_\psi \subset V_\varphi \tag{21}$$

since these responses can be represented using structural modal functions. The response functions ψ_i and excitation functions χ_i can be related by the integral

$$\psi_i(\mathbf{x}) = \int_\Omega g(\mathbf{x}|\mathbf{x}_0)\chi_i(\mathbf{x}_0)\, \mathrm{d}x_0\, \mathrm{d}y_0\, \mathrm{d}z_0, \tag{22}$$

where $g(\mathbf{x}|\mathbf{x}_0)$ is the Green's function relating the response at the location $(\mathbf{x})$ to an input located at $(\mathbf{x}_0)$ at a single frequency. With these definitions in place, it is now easier to illustrate under which conditions the ψ_i's are linearly independent.

Suppose functions $\psi_1, \psi_2, \ldots, \psi_n$ are linearly independent, but $\psi_1, \ldots, \psi_n, \psi_{n+1}$ are linearly dependent. With this assumption, one can write

$$\psi_{n+1} = k_1\psi_1 + k_2\psi_2 + \cdots + k_n\psi_n, \tag{23}$$

where k_i are again constants with at least one being nonzero. Substituting Eq. (22) into each term of Eq. (23) and collecting terms, the identity

$$\int_\Omega g(\mathbf{x}|\mathbf{x}_0)\left[\chi_{n+1}^0 - k_1\chi_1^0 - k_2\chi_2^0 - \cdots - k_n\chi_n^0\right] \mathrm{d}\Omega_0 \equiv 0 \tag{24}$$

is obtained. In this relation a shortened notation $\chi_i^0 = \chi_i(\mathbf{x}_0)$ is used. Eq. (24) illustrates that the Green's function g and the function $\chi_{n+1}^0 - k_1\chi_1^0 - k_2\chi_2^0 - \cdots - k_n\chi_n^0$ are orthogonal over the domain Ω regardless of the choice of $\mathbf{x}$. According to the reciprocity principle, $g(\mathbf{x}|\mathbf{x}_0) = g(\mathbf{x}_0|\mathbf{x})$. For a point force located at an arbitrary and non-fixed location $\mathbf{x}$, therefore, $g(\mathbf{x}_0|\mathbf{x})$ is interpreted as the response at $(\mathbf{x}_0)$. In general, this response due to this point force includes a summation over all of the basis functions of V_φ. Also depending on $\mathbf{x}$, the Green's function $g(\mathbf{x}|\mathbf{x}_0)$ can be any function in space V_φ. Suppose now that the force basis functions χ_i's are selected such that

$$\begin{aligned} \chi_1 &= \mathbf{r}_1^{\mathrm{T}} \begin{Bmatrix} \varphi_1 \\ \vdots \end{Bmatrix} + P_1, \\ &\vdots \\ \chi_{n+1} &= \mathbf{r}_{n+1}^{\mathrm{T}} \begin{Bmatrix} \varphi_1 \\ \vdots \end{Bmatrix} + P_{n+1}. \end{aligned} \tag{25}$$

The $n+1$ coefficient row vectors, $\mathbf{r}_i$, are required to be linearly independent, P_i is a function that is orthogonal to the response space, and $\{\varphi_1, \varphi_2, \ldots\}^{\mathrm{T}}$ includes an infinite number of mode shapes. In terms of a simply supported beam with a support at the origin, for example, $\{\varphi_1, \varphi_2, \ldots\}^{\mathrm{T}}$ includes the set of sine functions and P_i is a cosine function. Substituting Eq. (25) into Eq. (24), the identity established in Eq. (24) will be violated. This violation can be demonstrated by the observation that when Eq. (25) is substituted into Eq. (24), the integral on the left side of Eq. (25) is equal to

$$\int_\Omega g(\mathbf{x}|\mathbf{x}_0) \left[\mathbf{r}_{n+1}^{\mathrm{T}} \begin{Bmatrix} \varphi_1^0 \\ \vdots \end{Bmatrix} - k_1 \mathbf{r}_1^{\mathrm{T}} \begin{Bmatrix} \varphi_1^0 \\ \vdots \end{Bmatrix} \cdots - k_n \mathbf{r}_n^{\mathrm{T}} \begin{Bmatrix} \varphi_1 \\ \vdots \end{Bmatrix} \right] \mathrm{d}x_0 \, \mathrm{d}y_0 \, \mathrm{d}z_0$$

since each function P_i is orthogonal to the response space. In addition, if one considers the fact that $\mathbf{r}_i$ are linearly independent and the function $g(\mathbf{x}|\mathbf{x_0})$ includes a summation over all of the basis functions of V_φ, then the integral depends on $\mathbf{x}$ and is not always zero. Consequently, the Green's function and the series

$$\mathbf{r}_{n+1}^{\mathrm{T}} \begin{Bmatrix} \varphi_1^0 \\ \vdots \end{Bmatrix} - k_1 \mathbf{r}_1^{\mathrm{T}} \begin{Bmatrix} \varphi_1^0 \\ \vdots \end{Bmatrix} \cdots - k_n \mathbf{r}_n^{\mathrm{T}} \begin{Bmatrix} \varphi_1 \\ \vdots \end{Bmatrix}$$

cannot be orthogonal for different $\mathbf{x}$. Therefore, the initial assumption that the $(n+1)$ ψ_i's are linearly dependent is violated. Eq. (25) provides the conditions under which the forcing functions can be selected to guarantee the linear independence of the corresponding response functions. It is worth noting that since $\{\varphi_1, \varphi_2, \ldots\}^{\mathrm{T}}$ includes an infinite number of φ_i, $\mathbf{r}_i^{\mathrm{T}}$ also has an infinite number of elements. As a result the linear independence condition for the $\mathbf{r}_i$'s is possible to satisfy.

Although the conditions under which the linear independence of the response functions can be assured have been presented, which also guarantees that the $\mathbf{G}$ matrix can be inverted, there is still one implementation issue that needs to be addressed. This implementation issue is related to inverse instability that is associated with ill-posed problems. In the next section, methods for overcoming the inverse instability will be provided for a sample problem. Once that improvement

has been addressed, the actual numerical study for that same problem will be provided in a subsequent section.

5. Ill-posed problem and regularization method

Although the next section provides numerical results for a simple force reconstruction problem, it is useful to first consider the formulation for that problem so that the ill-posed nature of the new approach becomes evident. Furthermore, by understanding the ill-posed nature of the approach, a method for circumventing that issue can be developed. Then, the improvement will be used in the numerical study of the following section, to demonstrate its usefulness in stabilizing the force reconstruction solution.

Consider the case of a one-dimensional force reconstruction problem involving a simply supported beam excited by a distributed force, as shown in Fig. 2. The Green's function of the beam is given by [11]

$$g(x|x_0) = \frac{2}{M}\sum_{n=1}^{\infty}\frac{\sin(n\pi x_0/L)\sin(n\pi x/L)}{\omega^2-\omega_n^2}, \tag{26}$$

where

$$M = \rho_s s L \tag{27}$$

and

$$\omega_n = c_b\left(\frac{I}{s}\right)^{1/2}\left(\frac{n\pi}{L}\right)^2. \tag{28}$$

In these relationships, ρ_s denotes the density of the structural material, s is the cross section area of the beam, L is the length of the beam, and I is the second moment of area of the beam. The quantity c_b denotes the phase velocity of compressional waves in the beam

$$c_b = \left(\frac{E}{\rho_s}\right)^{1/2}, \tag{29}$$

where E is Young's modulus. Substituting Eq. (26) into Eq. (22), each response function $\psi_i(\mathbf{x})$ can be found to be

$$\psi_i(x) = \frac{2}{M}\sum_{n=1}^{\infty}\frac{\sin(n\pi x/L)}{\omega^2-\omega_n^2}\int_0^L \sin(n\pi x_0/L)\chi_i(x_0)\,\mathrm{d}x_0. \tag{30}$$

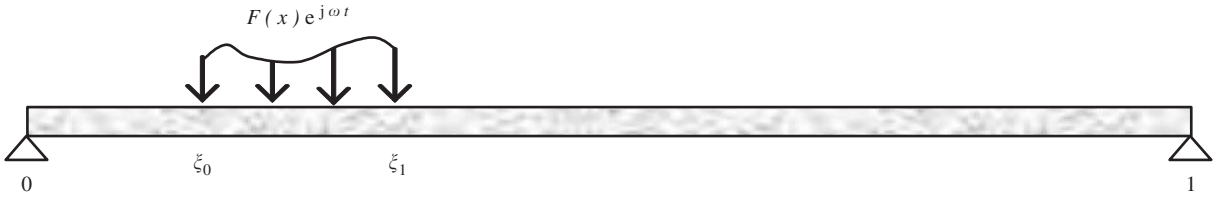

Fig. 2. Schematic of the beam problem.

Eq. (30) illustrates that $\psi_i(x)$ consists of an infinite number of structural modal functions. However, further examination of Eq. (30) shows that at a specific frequency, ψ_i consists mainly of a few dominant modal functions due to the fact that term $1/(\omega^2 - \omega_n^2)$ decays quickly with increasing difference between ω and ω_n. As ω approaches ω_n, $\psi_i(x)$ is dominated by only one mode

$$\psi_i(x) \approx \frac{2}{M} \cdot \frac{\sin(n\pi x/L)}{\omega^2 - \omega_n^2} \int_0^L \sin(n\pi x_0/L)\chi_i(x_0)\, \mathrm{d}x_0. \tag{31}$$

The lack of information provided by the absence of the other response functions, which will be clearly demonstrated in the numerical study provided below, results in the inverse equation shown in Eq. (14) being ill-conditioned. This ill-conditioned problem can be characterized as an ill-posed problem that is analogous to that defined in the field of mathematics [8]. The ill-posed nature ultimately leads to inverse instability. Note that this problem is also encountered in point force reconstruction methods [2,3]. To address the issue here and reduce any inversion instability, a regularization process is applied.

Based on the principle of the singular value decomposition (SVD) technique [12], the Gram matrix **G** takes the form

$$\mathbf{G} = \mathbf{U} \cdot \mathbf{\Sigma} \cdot \mathbf{V}^{\mathrm{H}}, \tag{32}$$

where **U** and **V** are unitary matrices (also called Hermitian orthogonal matrices), $\mathbf{V}^{\mathrm{H}}$ is the adjoint matrix of **V**, and Σ is a diagonal matrix whose elements are referred to as the singular values of matrix **G**. For the current case, Σ has the form

$$\mathbf{\Sigma} = \mathrm{diag}(s_1, \ldots, s_n), \tag{33}$$

where $s_1, s_2, \ldots, s_n$ are nonnegative singular values arranged in descending order, and diag(*) refers to a diagonal matrix with the elements in parentheses located on the main diagonal. According to Ref. [7], if

1. the singular values decay gradually to zero, and
2. the ratio between the largest and the smallest nonzero singular values is large,

that problem is called an ill-posed problem, which may lead to inverse instability. The inverse instability means, in terms of Eq. (14) for example, that any random errors in the **B** vector defined by Eq. (13) will be amplified if the discrete Picard condition [8] is satisfied. The discrete Picard condition states that if the coefficients $|\mathbf{u}_i^{\mathrm{T}}\mathbf{B}|$ on average decay to zero slower than the singular values s_i, then any random errors in **B** will be amplified. The vector $\mathbf{u}_i$ is the ith column vector of matrix **U**.

To overcome inversion instability, Pezerat and Guyader [13] proposed two regularization methods for the traditional modal force reconstruction method described earlier. These methods are the truncated SVD (TSVD) method and the R.I.F.F. method, which is an acronym for a French name that refers to a windowed filtered inverse regularization approach. In the present work, a more powerful regularization method, referred to as the Tikhonov method [8], will be proposed for increasing inverse stability in the new force reconstruction method. Note that the Tikhonov method is a continuous method in contrast with the discrete TSVD method. Although

this regularization method is widely used in other engineering applications, it has not been applied to distributed force reconstruction problems before.

The key idea in Tikhonov regularization is to incorporate an a priori assumption about the size and smoothness of the desired solution [8]. When applying this principle to the distributed force reconstruction problem, one is able to get the Tikhonov form

$$\min\left\{\|\mathbf{G}\mathbf{W}_\alpha - \mathbf{B}\|_2^2 + \alpha^2\|\mathbf{W}_\alpha\|_2^2\right\}, \tag{34}$$

where $\|\cdot\|_2$ denotes the second norm of the matrices, and $\mathbf{W}_\alpha$ denotes the regularized solution that is a function of the regularization parameter α. To select an optimum regularization parameter α, a convenient graphical tool, the L-curve method, is applied. The L-curve method involves a plot of the norm $\|\mathbf{W}_\alpha\|_2$ versus the corresponding residue norm $\|\mathbf{G}\mathbf{W}_\alpha - \mathbf{B}\|_2$ on a log–log scale. For most problems, the L-curve plot has an L-shaped appearance (hence its name) with a distinct corner separating the vertical and the horizontal parts of the curve. The corner of this curve represents the optimum regularization parameter α [7]. To accurately pinpoint the corner, Hansen proposed using the point of maximum curvature as the optimum regularization parameter. To obtain this point, define

$$X(\alpha) = \log\|\mathbf{G}\mathbf{W}_\alpha - \mathbf{B}\|_2^2$$

and

$$Y(\alpha) = \log\|\mathbf{W}_\alpha\|_2^2.$$

One selects the value of α that maximizes the curvature function

$$\kappa(\alpha) = \frac{X''(\alpha)Y'(\alpha) - X'(\alpha)Y''(\alpha)}{\left(X'(\alpha)^2 + Y'(\alpha)^2\right)^{3/2}}, \tag{35}$$

where $(')$ and $('')$ denote the first and second differentiation with respect to α, respectively.

6. Numerical simulation

To illustrate the application of this new force reconstruction method, including the use of the regularization method described in the previous section, a distributed force problem will be studied numerically in this section. First, both methods will be applied for the purpose of comparison. Then, white noise will be added into the simulated measurement response to study the impact of measurement errors. It will be shown, as noted above, that the inverse process is an ill-posed problem and therefore the noise is amplified. Finally, to address the error amplification associated with this inverse instability, the regularization method described above will be applied.

6.1. Comparison of methods

Consider a simply supported beam excited by a distributed dynamic force as shown in Fig. 2. The basic formulation for this system was given in Section 5. The geometry and material properties of the beam to be considered in the study are listed in Table 1. The first several natural frequencies of the beam, computed using Eq. (28), are listed in Table 2. Suppose that a distributed

dynamic force oscillating at 732 Hz, which is between the second and third natural frequency, is located between ξ_0 and ξ_1 as shown in Fig. 2. Here ξ_0 and ξ_1 are 0.2 and 0.3 m, respectively. In order to evaluate the effectiveness of the new spatial force reconstruction technique, the forcing basis functions, χ_i, first need to be selected. In this study, a series of Fourier functions are chosen as the basis functions such that

$$\chi_i(x) = \begin{cases} 1, & i = 0, \\ \cos\dfrac{2 \cdot i \cdot \pi \cdot (x - \xi_0)}{\xi_1 - \xi_0}, & i = 1 \cdots k, \\ \sin\dfrac{2 \cdot (i-k) \cdot \pi \cdot (x - \xi_0)}{\xi_1 - \xi_0}, & i = k+1 \cdots 2k \end{cases} \tag{36}$$

for $\xi_0 < x < \xi_1$,, and

$$\chi_i(x) = 0$$

otherwise. Decomposing these functions into structural modal functions, it can be shown that the basis functions in Eq. (36) satisfy the conditions such that the projection of the basis functions χ_i's into the space V_φ are linearly independent as specified in Eq. (25). To illustrate the advantages of this new force reconstruction approach over the traditional modal approach, two different cases will be studied numerically. These cases will be referred to as Cases A and B. In each study, experimentally measured data will be simulated using numerical results from an analytical solution. In the simulation conducted here, 60 modes were used to construct $\{\psi_i\}$ from Eq. (30). Once a discretized response is obtained using the analytical formulation, the **G** and **B** terms in Eq. (11) will be found via numerical integration (segment summation). In each case 101 evenly spaced points are used for each of the integrations. Although the integration results might degrade, fewer points can be used for the integration. In some of the studies discussed below, errors will be added to investigate the potential effects of measurement noise and modeling errors.

Case A consists of the reconstruction of a dynamic force distributed uniformly over the forcing region (e.g. a hat function) and at a driving frequency of 732 Hz. Both the new and traditional

Table 1
The geometry and material properties of a simply supported beam

Young's modulus, E (GPa)	206.8
Density, ρ_s (kg/m^3)	7820
Beam span, L (m)	1
Beam thickness (m)	0.05
Beam width (m)	0.05

Table 2
Selected computed natural frequencies

Mode number	1	2	3	4	5	6	7	8	9
Frequency (Hz)	117	466	1049	1866	2915	4197	5713	7462	9444

spatial force reconstruction methods are applied to indirectly calculate the characteristics of the driving dynamic force. Fig. 3 shows the reconstructed results computed from the new method and the previously discussed traditional modal method. Note for both methods, the beam is discretized and simulated response data from 101 points is used to compute reconstructed force. The new method, labeled "improved", incorporates one basis function to reconstruct the external forces. The traditional modal method, on the other hand, was used with 1, 10 and 100 basis functions to reconstruct the force. The figure demonstrates that for the new method, the reconstructed force is quite satisfactory. Although not illustrated here, the result computed from more basis functions will not change for the new modal method due to the fact that one of the basis functions matches the force distribution. For the traditional modal method with an increasing number of basis functions, the reconstructed result improves. However, even with 100 basis functions, the traditional modal method exhibits Gibbs phenomena near the discontinuous positions at $\xi_0 = 0.2$ and $\xi_1 = 0.3$. Obviously, the improved method works better here because one of the basis functions exactly matches the force distribution shape. Nevertheless, the fact that the basis functions in the improved method only extend over the forcing aperture also improves the accuracy. To examine these features in more detail, another case is considered.

Case B consists of a triangular-shaped distributed dynamic force at the driving frequency of 732 Hz. Again, both the new and traditional methods are applied to calculate the driving dynamic force from the response at 101 locations. The identified results are plotted in Fig. 4. This time, seven basis functions are used in the improved method, that is $k = 3$ as in Eq. (36). The reconstructed result found using the improved method is better than that for the traditional method with 100 basis functions, as the difference between the exact solution and that of the new method cannot be distinguished. In contrast, the reconstructed result found using the traditional modal method is not zero over the un-forced region.

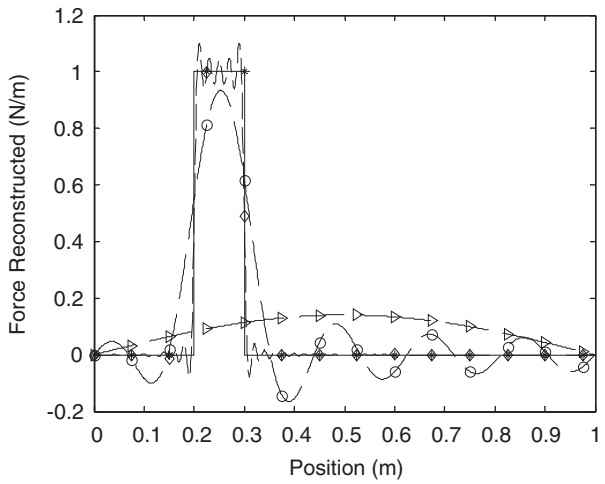

Fig. 3. Uniformly distributed force: comparison of the reconstructed results for the improved method (—∗—, one basis function used) and the traditional modal method (-▷-, one basis function used; -○-, 10 basis functions used; -◇-, 100 basis functions used). Note 101 points are used to compute these results.

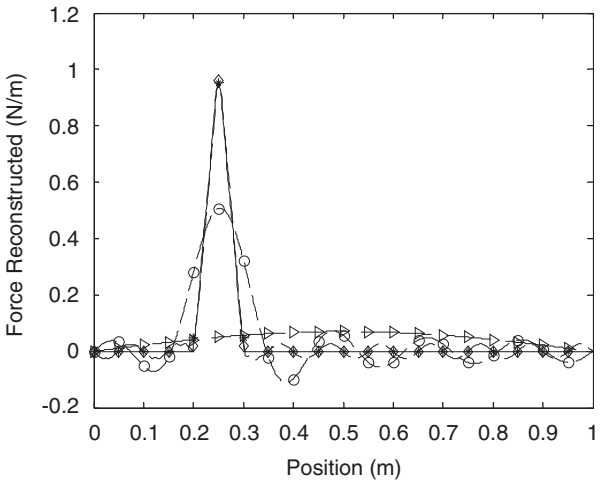

Fig. 4. Triangular-shaped distributed force comparison of the reconstructed results for the improved method (—∗—, seven basis function used) and the traditional modal method (—▷—, one basis function used; —○—, 10 basis functions used; —◇—, 100 basis functions used). Note 101 points are used to compute these results.

6.2. Application of the regularization method

From these two cases, one is able to conclude that in general, the new method is much more efficient than the traditional modal method. However, the new method also requires an inverse process (Eq. (14)) like the traditional modal method. Furthermore, a few of the structural modes tend to dominate some of the terms in the matrix **G**. As a result, the inverse of **G** might lead to error amplification problems as the dimension of **G** increases. This potential inverse issue is now examined.

Fig. 5 shows the singular values s_i for a Gram matrix **G** of size 15×15 to illustrate the trend of the singular values. Note in this plot, $k = 7$ in Eq. (36). Two observations can be made from the plot of singular values. First, the singular values of the Gram matrix **G** decay gradually to zero. Second, the ratio between the largest and the smallest nonzero singular values is 9.7×10^{15}. Based on these observations and the definition in the proceeding section, one is able to conclude that this problem is an ill-posed problem. Consequently, the results shown above may not be as good when noise is present in the measured response. Fig. 6 shows the singular values s_i, coefficients $\left|\mathbf{u}_i^{\mathrm{T}}\mathbf{B}\right|$, and the ratio $\left|\mathbf{u}_i^{\mathrm{T}}\mathbf{B}\right|/s_i$ for increasing i. In this figure, plot (a) illustrates these values when the response vector **B** given in Eq. (13) is not polluted by measurement error. That is, only errors associated with the simulation of the data are present. It is observed that the coefficients $\left|\mathbf{u}_i^{\mathrm{T}}\mathbf{B}\right|$ decrease faster than the singular values s_i. Hence the ratio $\left|\mathbf{u}_i^{\mathrm{T}}\mathbf{B}\right|/s_i$ is not increasing and a regularization method is not needed. Plot (b) illustrates these changes when the vector **B** is polluted by a Gaussian white noise with an arbitrarily chosen mean value of 5×10^{-8} and a standard deviation of 1. It is worth noting that the random noise is selected such that the norm of the noise is less than that of the exact signal. For the sample data generated here, the average signal to noise ratio is about 200. The plot shows that when the error is present in the **B** vector, the coefficients $\left|\mathbf{u}_i^{\mathrm{T}}\mathbf{B}\right|$ decrease slower than the singular values s_i. Hence the ratio $\left|\mathbf{u}_i^{\mathrm{T}}\mathbf{B}\right|/s_i$ is

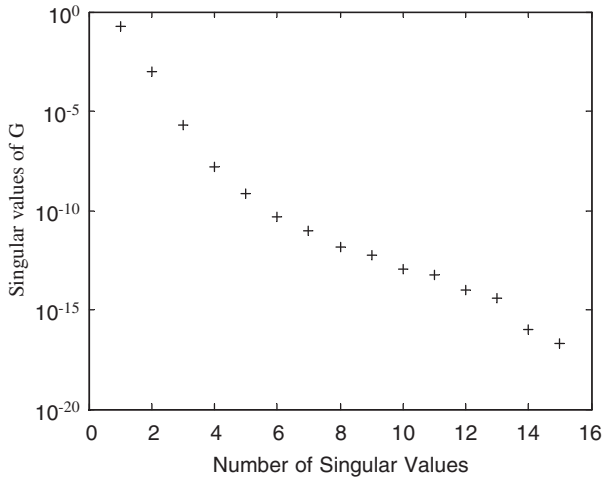

Fig. 5. Singular values of the Gram matrix **G**.

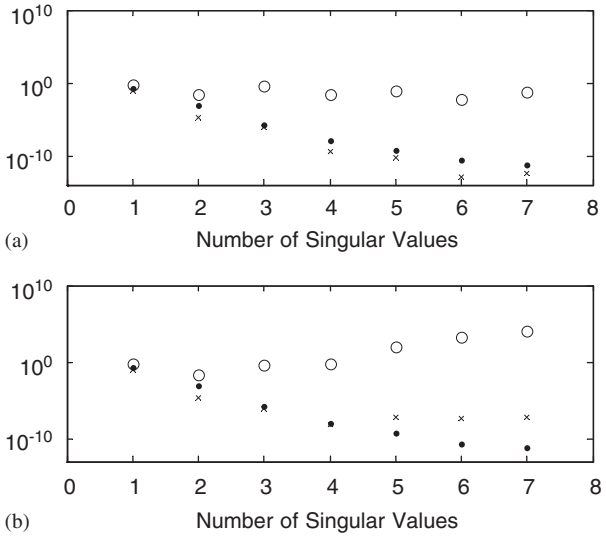

Fig. 6. Picard condition plot for (a) clean **B** vector and (b) polluted **B** vector ($\cdot$, singular value s_i; $\times$, $|\mathbf{u}_i^{\mathrm{T}}\mathbf{B}|$; $\circ$, $|\mathbf{u}_i^{\mathrm{T}}\mathbf{B}|/s_i$).

increasing. Based on the statement of the Picard condition, therefore, the error in the **B** vector will be amplified in the solution. Fig. 7 illustrates the reconstructed results computed from this polluted data according to the conditions stated above. As expected, the errors in **B** are widely amplified and propagate into the reconstructed forces.

To overcome this inversion issue of noise amplification, the regularization method described above is implemented. The L-curve for the Tikhonov regularization is plotted in Fig. 8 and the

optimum parameter of $\alpha = 1.06 \times 10^{-7}$ is computed using Eq. (35). Using this optimum parameter in the Tikhonov-based enhanced modal formulation, one is able to obtain the reconstructed force as plotted in Fig. 9. Clearly, the error amplification in the inverse process is significantly reduced and the reconstructed force matches the exact solution quite well. However, the peak of the exact solution is a little bit larger than that computed from the regularized method. This is due to the fact that the random errors are intermingled with the dynamic information. Hence the complete eradication of the random errors is not possible. It is also worth noting that

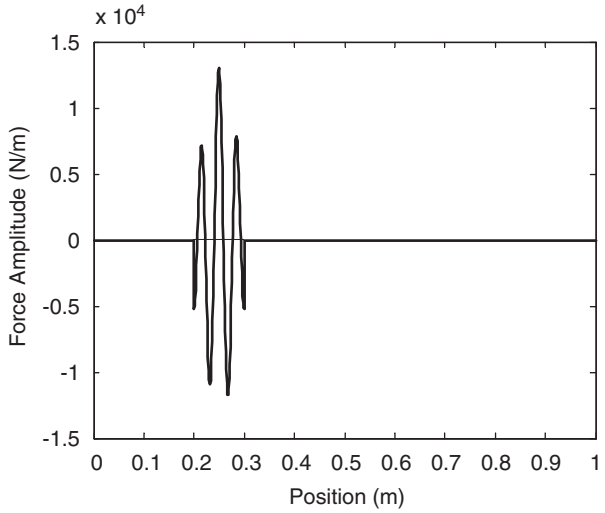

Fig. 7. Reconstructed triangle force with error present in **B** by using the improved method (——, exact force (peak = 1 N/m); ——, reconstructed force (peak = 13 000 N/m)). Note 101 points are used to compute these results.

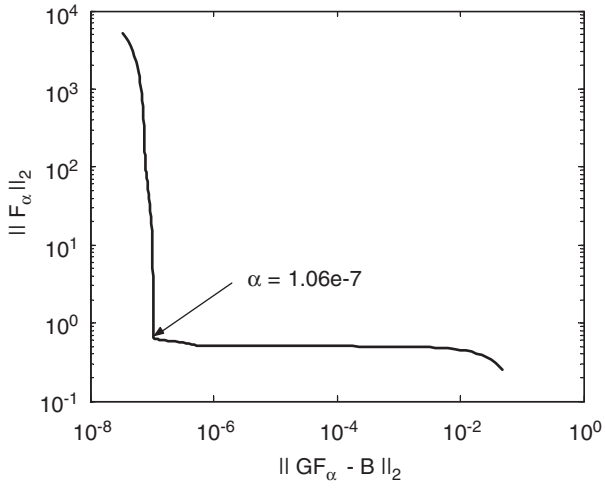

Fig. 8. L-curve plot for selection of optimal regularization parameter α.

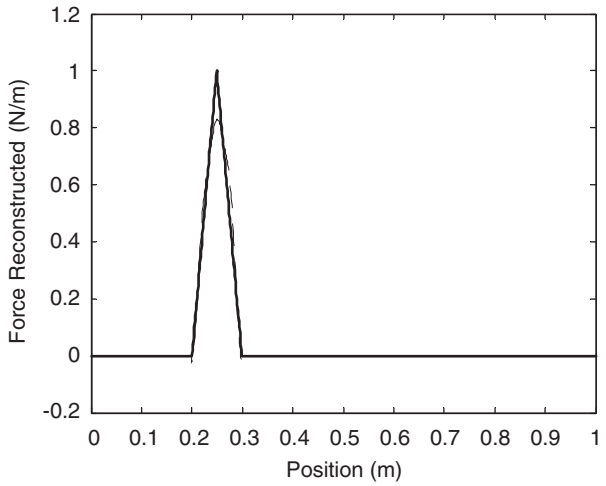

Fig. 9. Comparison between the regularized improved method and the exact solution (——, exact force (peak = 1 N/m); ——, reconstructed force). Note 101 points are used to compute these results.

the modal functions used here are assumed to be clean. If the actual modal functions are polluted, then $\{\psi_i\}$ are polluted and the matrix $\mathbf{G}$ will also be polluted. In this case, other regularization methods, such as total least square method, might be considered. Since the applicability of different regularization methods is beyond the scope of this work, such methods will be discussed in future papers.

7. Conclusion

This work presents a new force reconstruction method that can be used to determine spatially distributed dynamic forces from measured structural responses. Unlike the traditional modal force reconstruction method previously developed, where the forcing basis functions are defined over the entire structure, the new method requires that the basis functions only be defined over the finite region of the force. The new approach requires various selection criteria of the forcing basis functions to ensure linear independence of the associated response functions. When compared with the traditional modal method, both the theoretical and numerical studies show that this new method is much more efficient. Like the traditional modal method, the new method is also susceptible to an unstable inverse process that tends to amplify any random errors in the measured structural responses. It was shown that this inverse process belongs to the set of ill-posed problems. To deal with this problem, a Tikhonov regularization scheme was applied to reduce the effect of the error amplification. Additionally, in order to select the optimum parameter for the Tikhonov regularization, an L-curve principle was applied. Numerical studies show that the regularization process works well in conjunction with the new spatial force reconstruction method. The results of this study will be used in future experimental efforts.

Acknowledgements

This work was supported in part by the Center for Advanced Vehicle Technologies at The University of Alabama.

References

[1] K.K. Stevens, Force identification problems—an overview, *Proceedings of the SEM Spring Conference on Experimental Mechanics*, Houston, 1987.
[2] A.N. Thite, D.J. Thompson, The quantification of structure-borne transmission paths by inverse methods. Part 1: improved singular value rejection methods, *Journal of Sound and Vibration* 264 (2) (2003) 411–431.
[3] A.N. Thite, D.J. Thompson, The quantification of structure-borne transmission paths by inverse methods. Part 2: use of regularization techniques, *Journal of Sound and Vibration* 264 (2) (2003) 433–451.
[4] E. Jacquelin, A. Bennani, P. Hamelin, Force reconstruction: analysis and regularization of a deconvolution problem, *Journal of Sound and Vibration* 265 (1) (2003) 81–107.
[5] L. Cremer, M. Heckl, E.E. Ungar, *Structure-borne Sound: Structural Vibrations and Sound Radiation at Audio Frequencies*, Springer, Berlin, 1973.
[6] C. Pezerat, J.L. Guyader, Two inverse methods for localization of external sources exciting a beam, *Acta Acustica* 3 (1995) 1–10.
[7] P.C. Hansen, Regularization tools: a matlab package for analysis and solution of discrete ill-posed problems, *Numerical Algoritms* 6 (1994) 1–35.
[8] P.C. Hansen, *Rank-deficient and Discrete Ill-posed Problems*, SIAM, Philadelphia, 1998.
[9] L. Meirovitch, *Elements of Vibration Analysis*, McGraw-Hill, New York, 1975.
[10] S. Granger, L. Perotin, An inverse method for the identification of a distributed random excitation acting on a vibrating structure. Part 1: theory, *Mechanical Systems and Signal Processing* 13 (1999) 53–65.
[11] M.C. Junger, D. Feit, Sound, structures and their interactions, Acoustical Society of America, 1993.
[12] G.H. Golub, *Matrix Computation*, Johns Hopkins University Press, Baltimore, MD, 1996.
[13] C. Pezerat, J.L. Guyader, Force analysis technique: reconstruction of force distribution on plates, *Acustica* 86 (2000) 322–332.